Yang et al. Micro and Nano Systems Letters (2024) 12:8
https://doi.org/10.1186/s40486-024-00198-x

Micro and Nano Systems Letters

LETTER

Open Access

Exploring graphene structure, material properties, and electrochemical characteristics through laser-induced temperature analysis

Na-Kyoung Yang[1†], Yoo-Kyum Shin[2†], Saeyoung Park[1,2], Sang-Min Kim[2], Bon-Jae Koo[2], Joonsoo Jeong[1,2] and Min-Ho Seo[1,2*]

Abstract

Laser-induced graphene (LIG) is a three-dimensional graphene structure fabricated through the irradiation of a polymer substrate with laser energy (or fluence, equivalently). This methodology offers a cost-effective and facile means of producing 3D nanostructures, yielding graphene materials characterized by extremely high surface area and superior electrical properties, rendering them advantageous for various electrochemical applications. Nonetheless, it is imperative to acknowledge that the structures and material properties of LIG are subject to substantial variations contingent upon processing parameters, thereby underscoring the necessity for systematic inquiry and systematic comprehension of processing conditions, such as fluence and multi-passing, and resultant outcomes. Herein, we explored the impact of different laser fluence levels on the structural and material properties of LIG. We, especially, focused on how laser fluence affected substrate temperature and found that it caused polyimide (PI) substrate pyrolysis, resulting in changes in 3D structures and material density to LIG properties. We also investigated the effects of a multi-passing process on 3D LIG structures and material qualities, varying fluences, and temperature fluctuations. Lastly, we assessed electrochemical properties using LIGs produced under different conditions as working electrodes, leading to distinct impedance profiles and cyclic voltammetry (CV) curves. These variations were linked to the unique structural and material characteristics of the LIG samples.

Keywords Laser-induced graphene, Fluence, Temperature, Material properties

Introduction

Laser-induced graphene (LIG) is a three-dimensional porous graphene material generated by irradiating carbon-based materials with UV and CO_2 lasers in an atmospheric environment [1–3]. LIG offers several advantages that make it particularly appealing for various applications. It can be easily and rapidly manufactured using lasers, eliminating the need for expensive infrastructure like cleanroom facilities, which enhances its cost-effectiveness [4]. Furthermore, LIG boasts high design flexibility and can be crafted into intricate three-dimensional conductive micro- and nanostructures [5]. In addition to its ease of fabrication, LIG exhibits exceptional properties, including high electrical conductivity [6, 7], corrosion resistance [8], mechanical flexibility [9], and biocompatibility [10]. Moreover, its increased surface area due to its 3D porous micro- and nanostructure makes it highly attractive for applications in advanced electronic devices. LIG has garnered significant attention

†Na-Kyoung Yang and Yoo-Kyum Shin are contributed equally to this work.

*Correspondence:
Min-Ho Seo
mhseo@pusan.ac.kr
[1] School of Biomedical Convergence Engineering, Pusan National University, 49 Busandaehak-Ro, Mulgeum-Eup, Yangsan-Si, Gyeongsangnam-Do 50612, Republic of Korea
[2] Department of Information Convergence Engineering, Pusan National University, 49 Busandaehak-Ro, Mulgeum-Eup, Yangsan-Si, Gyeongsangnam-Do 50612, Republic of Korea

in recent years, especially in fields such as electronic skin [4], real-time physiological signal monitoring [11], and human–machine interaction [12].

Among its diverse applications, the use of LIG in electrochemical biosensors stands out due to its remarkable performance characteristics [13]. LIG, being based on highly conductive graphene, coupled with its 3D micro- and nano-porous structure, maximizes the available surface area. This unique feature allows for versatile surface functionalization, making it suitable for the development of highly sensitive electrochemical biosensors capable of selectively detecting a wide range of target substances. Since the recognition of LIG's potential as a biosensor material, extensive research efforts have been directed towards its optimization. Studies have focused not only on tailoring LIG's properties to detect specific substances but also on utilizing nanostructures for surface functionalization to broaden its detection capabilities [6, 14–16].

To achieve high-performance electrochemical biosensors utilizing LIG as electrodes, meticulous attention to the micro- and nanostructure and material properties of LIG is crucial. The extent to which the surface interacts with the target substance and the role of functionalized particles depend on the underlying LIG structure. Researchers have therefore dedicated significant efforts to experimentally fine-tune the three-dimensional structure, shape, and properties of LIG [17, 18]. This includes adjusting laser energy during LIG fabrication, as it directly impacts the heating and resultant graphene structure, but a comprehensive understanding of these processes is still evolving. Moreover, recent studies have explored the use of a multi-passing process to create high-quality LIG, however, a clear understanding of how variations in initial graphene morphology and laser energy conditions affect the resulting graphene properties remains limited [19]. This knowledge gap poses challenges when seeking to harness LIG for biosensor applications, highlighting the need for systematic research and analysis of LIG morphology and properties under various experimental conditions. Addressing these research gaps will not only enable the production of high-quality LIG but also provide essential insights for its application in biosensor technology. Moreover, it has the potential to expand the utility of LIG in future biosensor advancements, opening up exciting opportunities for its use in diverse fields.

In this study, we have undertaken a comprehensive exploration of the structural and material properties of LIGs with particular emphasis on the influence of varying laser fluence levels. Our investigations commenced with the fabrication of distinct LIG results, each characterized by unique structural and material attributes, achieved through the manipulation of laser fluence conditions. Our primary focus was directed towards scrutinizing the thermal effects induced by laser fluence on the substrate temperature. Experimental observations unequivocally affirmed that alterations in temperature (T) arising from the laser-induced process led to the pyrolysis of the polyimide (PI) substrate. This phenomenon resulted in a material melting and heightened material density and substantial modifications in the structural, surface, and material properties of the resultant LIGs. Subsequently, we conducted an in-depth examination of the impact of a multi-passing process, a technique that has garnered considerable attention among contemporary researchers. Our methodology involved the initial creation of stable 3D LIG structures, followed by the analysis of LIGs obtained through secondary laser treatments, each executed with varying fluences. Our analytical approach was further augmented by considering the temperature variations induced by the multi-passing process. This comprehensive analysis proved instrumental in elucidating our experimental findings. Lastly, our investigation extended to an assessment of the electrochemical properties exhibited by LIGs produced under diverse conditions. We harnessed LIGs fabricated under varying parameters as working electrodes, subjecting them to meticulous impedance and cyclic voltammetry measurements. The outcomes yielded distinctive impedance profiles and cyclic voltammetry curves for each set of electrodes. These variations were effectively expounded upon through a thorough examination of the structural and material characteristics inherent to the various LIG samples.

Results and discussion

To understand the structure and morphology of LIG formed based on the induced fluence (or energy, equivalently), we created LIG using a commercial CO_2 laser (VLS2.30DT, Universal: wavelength = 10.6 μm, laser power = 0–30 W, spot size = 70 μm, duration = 500 PPI, scan speed = 0–1270 mm/s, time interval = 4 s) and a commercially available 100-μm thick PI substrate (PIF-100, KESPI). As a result, we obtained a variety of 3D LIG structures and morphologies depending on the applied fluence. Figure 1a presents visual inspection data for representative LIG results produced at different fluences (E). (i) When the fluence was relatively low at 12.186 J/cm^2 (laser power: 7.5W, laser speed: 32 mm/s), we observed a slightly convex microstructure in three dimensions. The height (h), measured with a 3D profiler (VHX-7000, KEYENCE), was approximately 70 μm, with a defined width (w) by calculating the full width half maximum (FWHM) was approximately 150 μm (Fig. 1b). Cross-sectional scanning electron microscope (SEM) images revealed a slightly convex structure with micro-sized

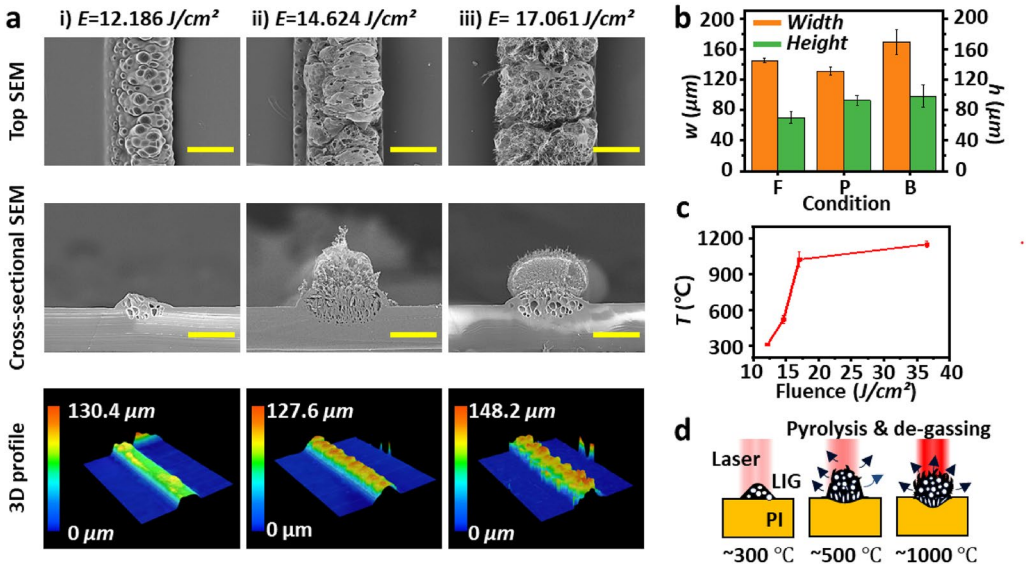

Fig. 1 Structural characterizations for single lasing LIGs. **a** SEM image and 3D profile image of LIGs according to laser fluence (*E*) 12.186 J/cm^2, 14.624 J/cm^2, and 17.061 J/cm^2 (scale bar:100 μm). **b** Width (*w*) and height (*h*) of LIGs according to Laser fluence 12.186, 14.624, and 17.061 J/cm^2. Each fluence is used to fabricate Foamy (F), Porous (P), and Bush (B) LIG (scale bar:100 μm). **c** Change of LIGs formation temperature according to laser fluence of 12.186, 14.624, 17.061, and 34.559 J/cm^2. **d** Schematic illustration of LIG formation process as laser fluence increased. Red mark means focused collimated light exposure

voids in the interior, contributing to its formation. However, the surface of the structure showed few voids. Therefore, we defined this result as the 'Foamy (*F*)' structure; (ii) Increasing the laser's fluences led to more three-dimensional and porous structures. At $E = 14.624$ J/cm^2 (laser power: 9W, laser speed: 32 mm/s), the height reached approximately 92 μm, with a width of approximately 137 μm (Fig. 1b). Upon closer examination through SEM images, we observed a convex-surfaced LIG structure interconnected internally with numerous micro- and nanoscale voids at surface and interior of the LIG structure, distinguishing it from the 'Foamy' structure. Thus, we termed this morphology as 'Porous (*P*)' structure; (iii) Lastly, at higher laser fluence, we noticed significant changes in the LIG's morphology once again. When an fluence (*E*) of 17.061 J/cm^2 (laser power: 10.5W, laser speed: 32 mm/s), was applied, we obtained a three-dimensional structure similar in height (approximately 98 μm) and width (approximately 137 μm) to the previous results. However, the surface appeared considerably rougher than before. This increased surface roughness led to a noticeable rise in the standard deviation of *h*, measured at 14.96 μm (Fig. 1b). This was significantly higher than the values of 7.48 μm for the 'Foamy' structure and 6.37 μm for the 'Porous' structure, respectively. The enhanced roughness observed in the SEM images was attributed to the formation of numerous graphene nanofibers on the surface. Therefore, we can classify this result as the 'Bush (*B*)' structure.

To elucidate the diversity in resulting morphologies based on the fluence input, we interpret our findings in terms of the variation in fluence-induced heat (or temperature) levels. According to the conventional Srinivasan-Smrtic-Babu (SSB) model, when a laser irradiates a polyimide (PI) substrate, changes in the substrate occur due to photo-chemical and photo-thermal reactions [20]. As fluence increases, the dominance of the photo-thermal phenomenon becomes evident, resulting in higher heat generation within the substrate [21]**.** Consequently, the morphology of the formed LIG can be altered significantly with increasing laser fluence and temperature (*T*). To experimentally confirm this, we measured noticeable temperature changes during laser processing using a commercial non-contact temperature sensor (CTvideo3MH2, OPTRIS). Figure 1c illustrates the heat generation in the polyimide substrate as a function of processing fluence. As the fluence increases by tens of J/cm^2, we can confirm the induced temperature rises up to ~ 1200 °C. Corresponding the induced temperature with the fabricated LIG structure and morphology, we can clearly understand the situation during the LIG formation. Notably, the 'Foamy', 'Porous', and 'Bush' structures were formed at approximately 300, 500, and 1000 °C, respectively. We can establish that stable three-dimensional LIG structures are achievable at temperatures exceeding 500 °C. This phenomenon can also be rationalized in the melting point of polyimide. As the processing temperature surpasses this threshold, the polyimide undergoes

pyrolysis and graphitization through the photothermal reaction, yielding copious gaseous byproducts. The escape of these gases (defined as "degassing") at temperatures above the melting point results in the pronounced three-dimensional structures and numerous surface voids observed. Given the typical melting point of polyimide, which is approximately 400 °C, our experimental results can be well understood with the proposed hypothesis. However, the structure height is not significantly changed in the Bush LIG from the Porous LIG, even though the induced temperature is drastically increased. Considering that the majority of structural transformations due to polyimide pyrolysis occur in the range of 400–500 °C, it explains the relatively minimal dimensional differences between LIG produced at temperatures exceeding 1000 °C and those at 500 °C. We also evaluated LIG fabrication at higher fluence levels. Structural analysis of LIG created with a fluence of 36.559 J/cm^2 also revealed a 'Bush' morphology. Our interpretation is supported by the measured temperature of approximately 1100 °C during processing at $E = 36.559$ J/cm^2, aligning closely with the claimed processing temperature for 'Bush' formation (~ 1000 °C). It's noteworthy that even at a relatively high fluence level of 36.559 J/cm^2, a temperature comparable to that at $F = 17.061$ J/cm^2 was attained, suggesting a trend akin to the photo-thermal reaction of polyimide as per the SSB model.

To assess not only the dimensional changes but also the material quality of the resulting LIG, we conducted Raman spectroscopy analysis. Figure 2a presents Raman spectra for three representative LIG structures obtained under different fluence conditions. For Foamy (F) LIG produced at a lower fluence level ($E = 12.186$ J/cm^2), we observed broad peaks at ~ 1300, 1600, and 2700 cm^{-1}, which are expected to correspond to the D, G, and 2D peaks of conventional graphene, respectively. In contrast, for the more three-dimensional 'Porous (P)' and 'Bush (B)' LIGs fabricated at relatively higher energies, sharp peaks were also observed at ~ 1300, 1600, and 2700 cm^{-1}, aligning with the D, G, and 2D peaks, respectively. For quantitative analysis, we extracted the I_D/I_G ratio for each LIG (Fig. 2b). While it was challenging to determine this ratio precisely for the Foamy LIG due to the broad peaks, we obtained I_D/I_G values of approximately 0.93 and 0.9 for 'Porous' and 'Bush' LIGs, respectively. Statistical analysis across multiple samples (n = 3) revealed no significant difference between these two conditions. Additionally, we calculated the crystalline size of LIG structures (Fig. 2c). The calculated crystalline size was approximately 20 nm for both 'Porous' and 'Bush' LIGs. This implies that despite using higher fluence, and thus higher temperature, to create LIG, the crystal size does not significantly increase. Finally, we compared the I_{2D}/I_G values derived from the Raman spectra. Although determining this value for Foamy LIG remained challenging, 'Porous' and 'Bush' LIGs exhibited values of 0.65 and 0.37, respectively. These values suggest that 'Porous' LIG consists of few-layer graphene, while 'Bush' LIG is composed of multi-layer graphene. This interpretation aligns with the effect of higher laser fluence and temperature, which leads to further pyrolysis, resulting in a denser graphene structure.

Thus far, we have examined the impact of varying laser process fluence on the structural, morphological, and material properties of the fabricated LIG. Our comprehensive analysis reveals that when processed at temperatures below the polyimide melting point, LIG structures exhibit only slight convexity with internal voids, lacking the desired high three-dimensional characteristics and material quality. However, when subjected to temperatures exceeding 500 °C, we can attain high-quality three-dimensional graphene structures, with the added advantage of controlling their surface morphology by adjusting the fluence levels.

More recently, there have been active researches on modifying the structural and material properties of LIG

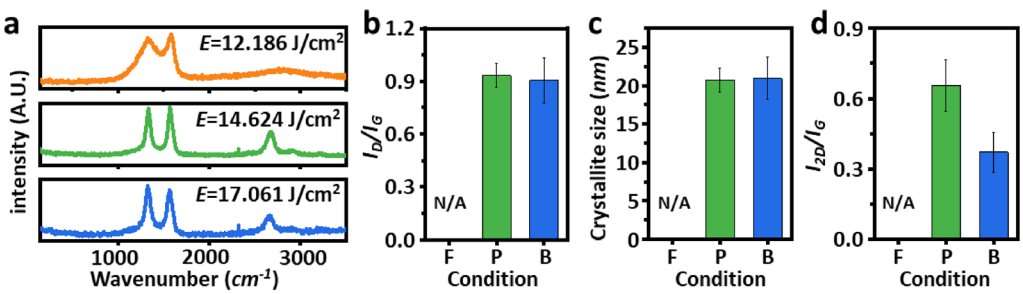

Fig. 2 Material quality analysis using Raman spectrum. **a** Raman spectrum of Foamy, Porous, and Bush LIGs produced by 12.186, 14.624, and 17.061 J/cm^2, respectively. **b**–**d** Extracted I_D/I_G (**b**), crystalline size (**c**), and I_{2D}/I_G (**d**) according to shape of LIG made by various fluence conditions

through multi-pass laser processing [19]. In this regard, we aimed to further analyze the structural and material changes in LIG induced by multi-passing. To do this, we initially defined the first pass Porous (P) LIG as a reference, which exhibited stable structure and excellent material properties. Subsequently, we applied additional fluences of 12.186, 14.624, and 17.061 J/cm^2 (the same fluences used for creating Foamy (F) LIG, Porous (P) LIG, and Bush (B) LIG, respectively) as secondary passes to the 1st pass Porous LIG. The obtained surface and cross-sectional SEM images are shown in Fig. 3a, b. When the 2nd laser pass was applied, it is ambiguous to define the width of the produced LIG structures across all conditions. However, it is evident that the resulting LIG structures resembled the Bush LIG on the surface (Fig. 3a, b). To make a clear dimensional comparison of the obtained LIGs, we extracted the heights (h) of LIG structures at nine different points and calculated the averages. As a result, for 2nd laser fluences of 12.186, 14.624, and 17.061 J/cm^2, the heights were measured as $h = 40.40$ µm ($E = 12.186$ J/cm^2), $h = 29.61$ µm ($E = 14.624$ J/cm^2), and $h = 45.54$ µm ($E = 17.061$ J/cm^2), respectively. These heights represent a noticeable decrease compared to the initial 3D structures (Fig. 3c). This significant change is attributed to the thermal decomposition of graphite. For a more detailed explanation, we measured the sample's temperature during the 2nd laser pass, revealing that regardless of the applied fluence, temperatures (T) consistently exceeded 1200–1300 °C. Typically, it is well known that conventional graphite undergoes thermal decomposition around 1000 °C, and the high temperature generated during the 2nd laser pass led to the decomposition of multi-layer graphene (or graphite) already present in the LIG, resulting in significant volume and surface changes [22].

To further understand these processes, we analyzed the Raman spectrum of LIG during this phase. Figures 3e–g display the I_D/I_G, crystalline size, and I_{2D}/I_G results for 1st pass Porous LIG and 2nd pass Bush LIG. Notably, there were no significant differences in properties between the Porous LIG obtained from the 1st laser pass and the Bush LIG produced through multi-passing. This experimental evidence highlights that while they share structural similarities through multi-passing, they yield LIGs with different material properties (layers) compared to the Bush LIG obtained from the 1st laser pass.

Finally, we further investigate on electro-chemical properties of the LIGs fabricated with applied fluence and multi-pass. To evaluate the electro-chemical properties of various LIGs produced under different conditions

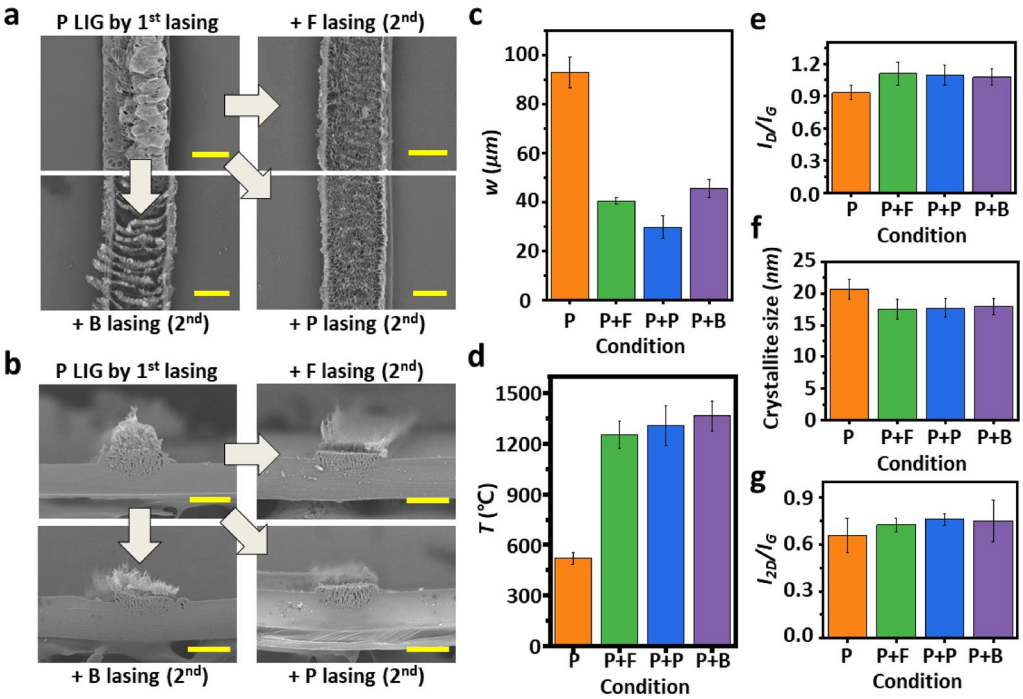

Fig. 3 Characterizations for LIG fabricated by multi-pass process. **a** Top view SEM images of fabricated LIG before and after second lasing with different fluence by 12.186 (F), 14.624 (P), and 17.061 (B) J/cm^2 (scale bar:100 µm). **b** Cross-sectional SEM image of LIGs before and after second lasing with different fluence (12.186, 14.624, and 17.061 J/cm^2) (scale bar:100 µm). **c** height (h) of LIGs fabricated with various condition, **d** Measured induced temperature by the 2nd lasing. **e**–**g** Material property changes, including I_D/I_G (**e**), crystalline size (**f**), and I_{2D}/I_G (**g**), by the 2nd lasing

and methods, we fabricated LIG electrodes with an 8 mm diameter in a working electrode configuration (Fig. 4a, b). We secured a conventional metal wire to the LIG using silver (Ag) paste and immersed them in a pH = 7.4 phosphate buffer solution (PBS), alongside commercial platinum (Pt) counter electrodes and Ag/AgCl reference electrodes. We conducted impedance and cyclic voltammetry (CV) measurements using a potentiostat in the traditional three-electrode setup (Fig. 4c). CVs recorded in a potential window of (−0.2 V to 0.4 V) vs Ag/AgCl with a scan rate of 10 mV/s in 0.1 M phosphate Buffer (pH 7.4) at 10 mM Ferrocene. The impedance results for each electrode are presented in Figs. 4d, e, showing typical impedance (Z) characteristics across the frequency range of 1 to 10^6 Hz. To facilitate comparison, impedance values at 1 kHz were extracted. A comparison was made between Foamy, Porous, and Bush LIG electrodes produced using a single laser pass with different energy levels. It was observed that Foamy electrodes exhibited poor electrochemical characteristics, while Porous LIG electrodes displayed approximately 750 Ω and Bush LIG electrodes showed around 600 Ω. This difference can be attributed to the higher surface area of Bush LIG, which features more surface porosity despite having similar dimensional properties.

The CV characteristics of both electrodes were also compared (Fig. 4f, g). Both electrodes exhibited similar CV shapes during dual-sweep measurements from −0.2 to 0.4 V. However, the Porous LIG electrode (A = 15.58W) exhibited a larger area (A) in the measured CV curve, compared to the Bush LIG electrode (A = 11.52W). CV curve area is calculated by a function of 'Polygon Area' in a commercial software, Origin (2022b, Originlab). This result can be understood in terms of surface activity; thinner layers of graphene, as in Porous LIG, typically exhibit higher surface activity than thicker layers of graphene, as in Bush LIG, as corroborated by the analysis in Fig. 2d.

We also conducted an analysis of LIG electrode results obtained through multi-passing process (Fig. 4h), using the same conditions as in Fig. 3. These electrodes exhibited typical impedance characteristics across all frequency ranges, but there were noticeable differences in impedance levels among the samples. To quantitatively

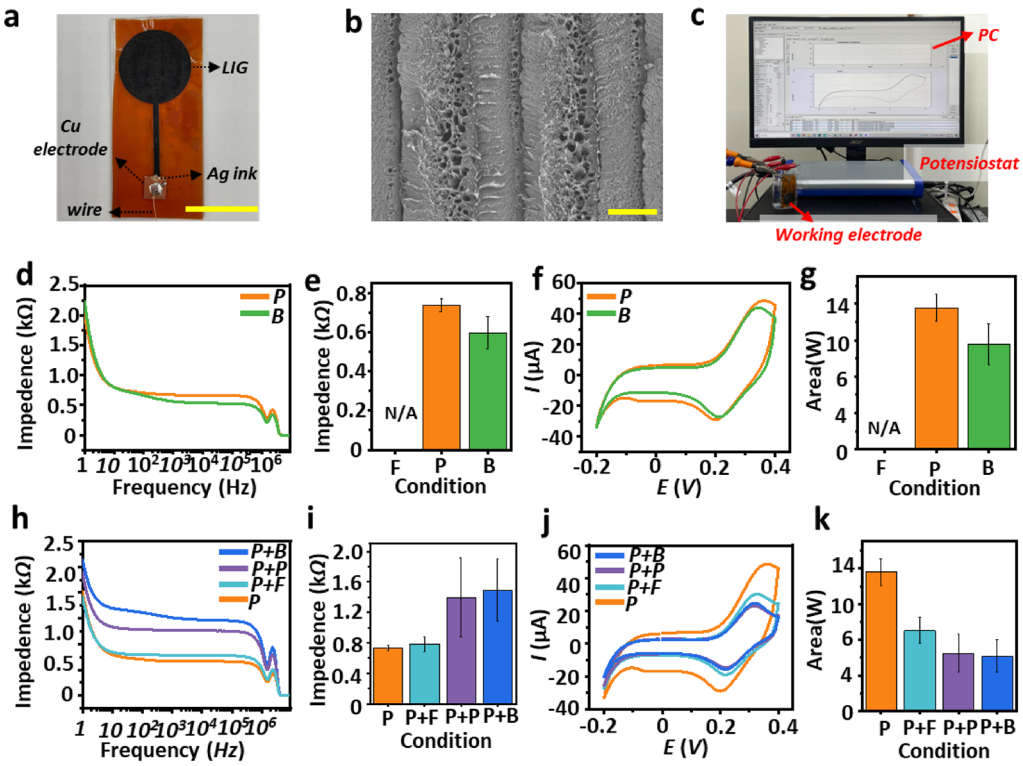

Fig. 4 Electrochemical characterization of fabricated LIG working electrode. **a** Photograph of the fabricated LIG working electrode (scale bar = 20 mm), **b** Top SEM image of the LIG electrode (scale bar:100 μm). **c** Photograph of experimental set-up. **d** Measured impedance and frequency curve of different types of LIGs. **e** Extracted impedance (@1 kHz) of LIGs fabricated by Porous (P) and Bush (B) conditions. f) CV curve of different type of LIGs. **g** Extracted CV curve area of P and B type of LIG. **h** Impedance-frequency curve of LIGs fabricated by the different 2nd lasing condition. **i** Comparison of the extracted impedance of various LIGs. **j** CV curve of various LIGs fabricated by the 2nd lasing process. **k** Extracted CV curve area of various LIGs

compare these results, impedance values at 1 kHz were extracted, revealing that multi-passed LIG generally exhibited higher impedance compared to 1st pass Porous LIG ($Z=750$, 1400, and 1500 Ω for Porous + Foamy ($P+F$), Porous + Porous ($P+P$), and Porous + Bush ($P+B$) conditions, respectively) (Fig. 4i). Notably, a significant increase in impedance was observed with higher fluences during the 2nd laser pass. This can be attributed to the decomposition of a substantial amount of graphene during the 2nd laser pass, resulting in a surface rich in porosity but a reduction in the overall reactive surface area. These impedance results were consistent with the CV characteristics of the electrodes (Fig. 4j). All electrodes exhibited similar CV shapes. However, as the multi-passing process and 2nd laser pass fluence increased, a reduction in CV area (A) was observed (Fig. 4k). This reduction in area of CV curves suggests that even for electrodes with similar material properties (graphene layers), a decrease in surface area that also contribute to electro-chemical reaction was observed due to the thermal decomposition during the multi-passing process.

Conclusion

In this comprehensive study, we delved into the structural, morphological, and material properties of LIG, with a primary focus on the influence of varying laser fluence levels. We summarize the properties of LIG depending on the laser's fluence and effect of 2nd laser for each condition (Table 1). Our investigations led to several significant findings and insights: (1) Thermal Effects on structure and material quality: We demonstrated that alterations in laser fluence levels significantly impacted the structural and morphological properties of LIG. At temperatures below the polyimide melting point, low quality of LIG fabricated, exhibiting relatively simple, slightly convex structures with internal voids. In contrast, temperatures exceeding 500 °C resulted in the formation of high-quality, three-dimensional graphene structures. Moreover, when the temperature exceeds 1000 °C, the fabricated LIG also shows high-quality, three-dimensional structure, but with intricate surface morphologies, such as the 'Bush' structure. These findings highlighted the crucial role of temperature in LIG fabrication; (2) Multi-Passing Effects: Our exploration of multi-pass laser processing revealed that secondary laser passes, applied with varying fluences, led to structural transformations in LIG. The reduced heights of the fabricated LIG are experimentally confirmed after the 2nd lasing processes regardless of fluence, but all results show closely resembled the 'Bush' LIG obtained from the first laser. These structural changes were attributed to the thermal decomposition of multi-layer graphene already present in the Porous LIG; (3) Material Quality: Raman spectroscopy analysis provided insights into the material quality of LIG. We found that LIG produced through the through multi-passing maintained similar material properties (layers) compared to LIG created in the initial pass. This indicated that the material quality remained consistent even when subject to additional laser processing; and (4) Electrochemical properties: Evaluation of LIG's electrochemical properties revealed that LIG electrodes exhibited distinct impedance profiles and cyclic voltammetry (CV) curves. While 'Foamy' LIG exhibited poor electrochemical characteristics, 'Porous' and 'Bush' LIG electrodes displayed improved performance. 'Porous' LIG, with thinner graphene layers, exhibited higher surface activity and a larger CV area compared to 'Bush' LIG. Multi-passed LIG, on the other hand, showed higher impedance and reduced CV areas due to thermal decomposition and surface area degradation during the multi-passing process.

In summary, we investigate the results (structures and properties) of LIG produced under different conditions of the CO_2 laser (fluence, multi-passing) in relation to temperature and perform an evaluation of the electrochemical properties of LIG created under various conditions. These insights provide valuable guidance for

Table 1 Summarize properties of LIG depending on laser's fluence and second lasing fluence

	F	P	B	P + F	P + P	P + B
1st fluence (J/cm^2)	12.2	14.6	17.1	14.6	14.6	14.6
2nd fluence (J/cm^2)	–	–	–	12.2	14.6	17.1
Height (μm)	69.9	92.9	98.3	40.4	29.6	45.5
Width (μm)	144.9	130.9	169.5	–	–	–
Temperature (°C)	478.1	653.6	1030.4	1255.0	1308	1365.9
I_D/I_G	–	0.932	0.932	1.107	1.092	1.077
Crystallite size (nm)	–	20.7	20.9	17.5	17.7	17.9
I_{2D}/I_G	–	0.655	0.370	0.724	0.759	0.749

tailoring LIG structures and properties for various applications, including electrochemical biosensors, electronic devices, and beyond. Future research in this field should continue to explore the potential of LIG while considering the intricate relationships between laser parameters and material characteristics.

Acknowledgements
This research was supported by 2022 BK21 FOUR Program of Pusan National University.

Author contributions
NKY and YKS: Conceptualization, figure preparation, experiment design, data analysis, visualization, writing; SP: Experiment design and measurement; SMK and BJK: Measurement and visualization; JJ: Measurement; MHS: Methodology, supervision, writing–review and editing. All the authors have read and approved the final version of the manuscript.

Funding
Not applicable.

Availability of data and materials
All data generated or analyzed during this study are included in this published article.

Declarations

Ethics approval and consent to participate
The authors declare that they have no competing interests.

Consent for publication
Authors consent the Springer Open license agreement to publish the article.

Competing interests
The authors declare that they have no competing interests.

Received: 7 February 2024 Accepted: 17 February 2024
Published online: 27 February 2024

References

1. Lin J et al (2014) Laser-induced porous graphene films from commercial polymers. Nat Commun 5:5714
2. Ma W, Zhu J, Wang Z, Song W, Cao G (2020) Recent advances in preparation and application of laser-induced graphene in energy storage devices. Mater Today Energy 18:100569
3. Ye R, James DK, Tour JM (2019) Laser-induced graphene: from discovery to translation. Adv Mater 31:e1803621
4. Wang H, Zhao Z, Liu P, Guo X (2022) Laser-induced graphene based flexible electronic devices. Biosensors (Basel) 12:55
5. Le TS et al (2022) Recent advances in laser-induced graphene: mechanism, fabrication, properties, and applications in flexible electronics. Adv Funct Mater 32:2205158
6. Liu J et al (2022) Laser-induced graphene (LIG)-driven medical sensors for health monitoring and diseases diagnosis. Mikrochim Acta 189:54
7. Zhang Q et al (2016) Human-like sensing and reflexes of graphene-based films. Adv Sci (Weinh) 3:1600130
8. Khan MA, Hristovski IR, Marinaro G, Kosel J (2017) Magnetic composite hydrodynamic pump with laser-induced graphene electrodes. IEEE Trans Magn 53:1–4
9. Han T et al (2019) Multifunctional flexible sensor based on laser-induced graphene. Sensors (Basel) 19:3477
10. Correia R et al (2022) Biocompatible parylene-C laser-induced graphene electrodes for microsupercapacitor applications. ACS Appl Mater Interfaces 14:46427–46438
11. Gandla S et al (2020) Highly linear and stable flexible temperature sensors based on laser-induced carbonization of polyimide substrates for personal mobile monitoring. Adv Mater Technol 5:2000014
12. Zou Y et al (2023) Flexible wearable strain sensors based on laser-induced graphene for monitoring human physiological signals. Polymers (Basel) 15:3553
13. Wan Z, Nguyen N-T, Gao Y, Li Q (2020) Laser induced graphene for biosensors. Sustain Mater Technol 25:e00205
14. Settu K, Chiu PT, Huang YM (2021) Laser-induced graphene-based enzymatic biosensor for glucose detection. Polymers (Basel) 13:2795
15. Xu Y et al (2021) Laser-induced graphene for bioelectronics and soft actuators. Nano Res 14:3033–3050
16. Zhu J et al (2021) Laser-induced graphene non-enzymatic glucose sensors for on-body measurements. Biosens Bioelectron 193:113606
17. Thakur AK, Lin B, Nowrin FH, Malmali M (2021) Comparing structure and sorption characteristics of laser-induced graphene (LIG) from various polymeric substrates. ACS ES&T Water 2:75–87
18. Vivaldi FM et al (2021) Three-dimensional (3D) laser-induced graphene: structure, properties, and application to chemical sensing. ACS Appl Mater Interfaces 13:30245–30260
19. Kaur S, Mager D, Korvink JG, Islam M (2021) Unraveling the dependency on multiple passes in laser-induced graphene electrodes for supercapacitor and H2O2 sensing. Mater Sci Energy Technol 4:407–412
20. Hong S, Kim J, Jung S, Lee J, Shin BS (2023) Surface morphological growth characteristics of laser-induced graphene with UV pulsed laser and sensor applications. ACS Mater Lett 5:1261–1270
21. Shin BS, Oh JY, Sohn H (2007) Theoretical and experimental investigations into laser ablation of polyimide and copper films with 355-nm Nd:YVO4 laser. J Mater Process Technol 187–188:260–263
22. Lim YJ, Heo JI, Madou M, Shin HJ (2013) Monolithic carbon structures including suspended single nanowires and nanomeshes as a sensor platform. Nanoscale Res Lett 8:492

Publisher's Note